96-506

E9-96-506

S.B.Vorozhtsov, D.V.Altiparmakov*

SIMULATION OF THE MAGNETIC FIELD
OF THE **VINCY** CYCLOTRON

*VINCA Institute of Nuclear Sciences, Belgrade, Yugoslavia
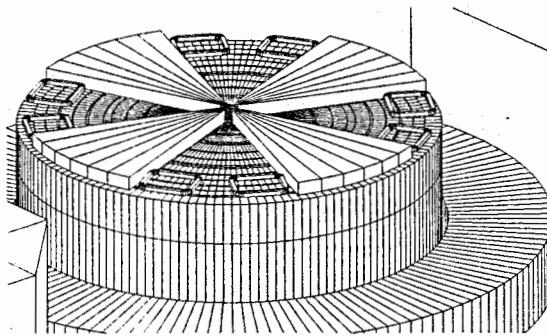
1996

Figure 1: VINCY Cyclotron Magnet Configuration.

Introduction. The VINCY Cyclotron is the main part of the TESLA Accelerator Installation, whose construction is under way in the VINCA Institute of Nuclear Sciences [1]. It is a multipurpose isochronous cyclotron with four straight sectors, designed to accelerate a wide range of ions ($\approx$ 20 μA of 73 MeV deuterons, $\approx$ 2 μA of 66 MeV protons, heavy ions of lower energy, etc). Various aspects of the system are shown schematically in Fig. 1. There, one can see the vertical yokes, pole disk, central plug, 4 sector shims, pole, main coil, harmonic and trim coils.

To determine the operating range [2] of the cyclotron 2D computation of the median plane field by the POISCR code and 3D computation by the TOSCA code were performed. The 2D results were used to study various designs of shimming elements.
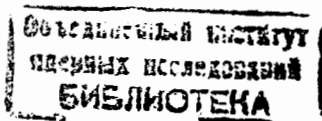
In this paper the 3D method is mostly considered [3]. This method was used to perform a cross-check for the 2D methods, to get new information on the field, which could not be obtained with the 2D calculations, and to contribute to the magnetic system design and shimming concept.

Calculation Tasks. The following aspects of the system were considered: the field in the acceleration region, the extraction region and the stray field distributions; comparison of the calculations with the measurements on the magnet model; ponderomotive forces; trim and harmonic coil field contributions; the lower axial channel magnetic field.

Median Plane Field. For the first set of calculations the so-called simplified model with and without sectors was chosen. There, some simplifications were adopted for the geometry of the magnet.

The data on the magnetization curve within the above mentioned VINCY cyclotron magnetic model are presented in Fig. 2. The calculations show rather bad $\approx$ 40 % efficiency of the magnet ($\approx$ 60 % of the total amperturns just wasted to overcome magnetic resistance of iron), which leads to relatively large power consumption.

The midplane field distributions for the main coil current of 600 A are presented in
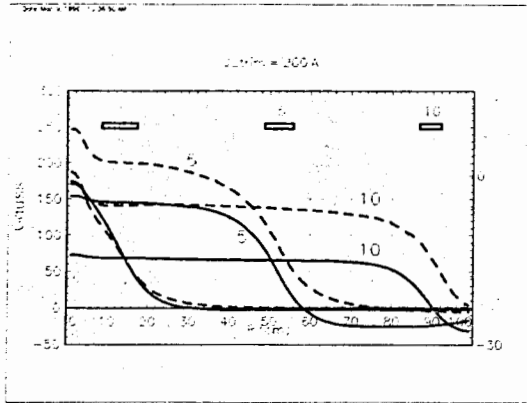
Figure 5: Mean field contribution from trim coils No 1, 5, 10. The dashed lines are for the main coil current 250 A, the solid lines are for 600 A.

form of the sector shims in the 2D models instead of their tapered form in reality.

The 3D calculations for the trim coils in the very center, in the middle of the radial range, and near the final radius were performed. In Fig. 5 the azimuthal averaged coil field contributions are shown. There is quite noticeable trim coil response dependence on the magnet field level. The more saturation of the ferromagnetic elements, the less the trim coil field contribution.

The comparison of the 3D calculations with the 2D results (Fig. 6) shows good agreement, except some difference in the radial gradients (3D gradients are about 20 % smaller than the 2D ones) and the very center region bump values.

The 3D nature of the calculations manifests itself in the azimuthal variation of the coil field response. This effect causes distortion of the 4th and 8th harmonics due to the trim coils being on. But the modification of these harmonics is rather small ($\leq$ 40 Gauss) as compared with the tolerance, imposed by the beam dynamics.

Harmonic Coils. Firstly, the harmonic coil field contribution was obtained, assuming only the conductor field. The magnet core had a simplified configuration with infinite permeability. To take into account the field contribution from the magnet core a set the coil reflections in around the iron surface was performed. This model (method 1) could lead to some systematic error in the results.

Then, the latest 3D TOSCA magnet model was used for the 3D simulation in the very center and near the final radius (method 2). The main coil current was 600 A, the harmonic coil current was 200 A. The coil configuration was just a simplified version of the real one, proposed for the design. But it retained all the features of the real coil to check its response field at the full extent. For example, the central region coil is situated
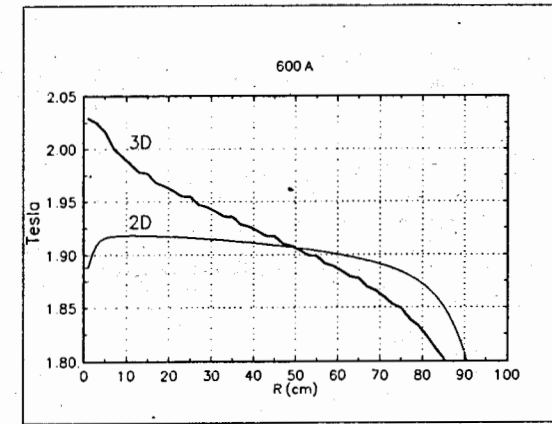

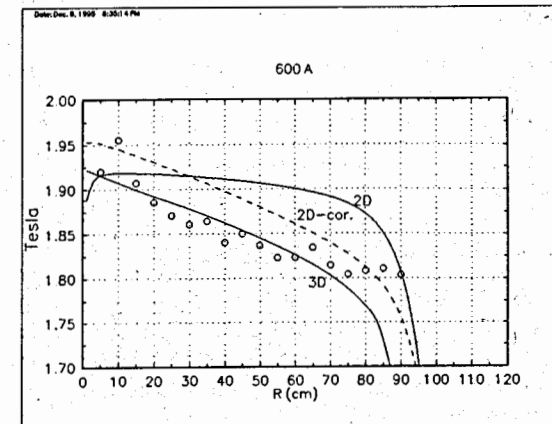Figure 3: Mean field radial dependence for 2D and 3D models.

Figure 4: Solid lines are 2D and 3D calculations, circles are measurements, the dash line is the 2D calculation with the 3D correction.
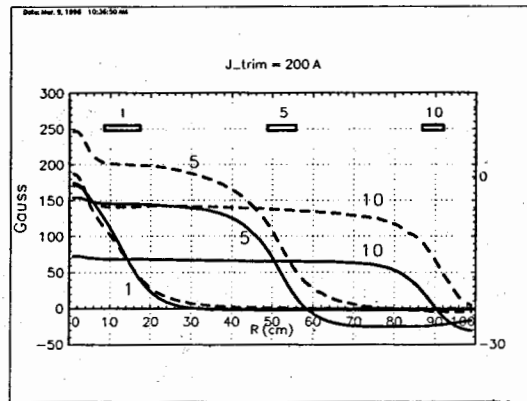
Figure 5: Mean field contribution from trim coils No 1, 5, 10. The dashed lines are for the main coil current 250 A, the solid lines are for 600 A.

form of the sector shims in the 2D models instead of their tapered form in reality.

The 3D calculations for the trim coils in the very center, in the middle of the radial range, and near the final radius were performed. In Fig. 5 the azimuthal averaged coil field contributions are shown. There is quite noticeable trim coil response dependence on the magnet field level. The more saturation of the ferromagnetic elements, the less the trim coil field contribution.

The comparison of the 3D calculations with the 2D results (Fig. 6) shows good agreement, except some difference in the radial gradients (3D gradients are about 20 % smaller than the 2D ones) and the very center region bump values.

The 3D nature of the calculations manifests itself in the azimuthal variation of the coil field response. This effect causes distortion of the 4th and 8th harmonics due to the trim coils being on. But the modification of these harmonics is rather small ($\leq$ 40 Gauss) as compared with the tolerance, imposed by the beam dynamics.

Harmonic Coils. Firstly, the harmonic coil field contribution was obtained, assuming only the conductor field. The magnet core had a simplified configuration with infinite permeability. To take into account the field contribution from the magnet core a set the coil reflections in around the iron surface was performed. This model (method 1) could lead to some systematic error in the results.

Then, the latest 3D TOSCA magnet model was used for the 3D simulation in the very center and near the final radius (method 2). The main coil current was 600 A, the harmonic coil current was 200 A. The coil configuration was just a simplified version of the real one, proposed for the design. But it retained all the features of the real coil to check its response field at the full extent. For example, the central region coil is situated
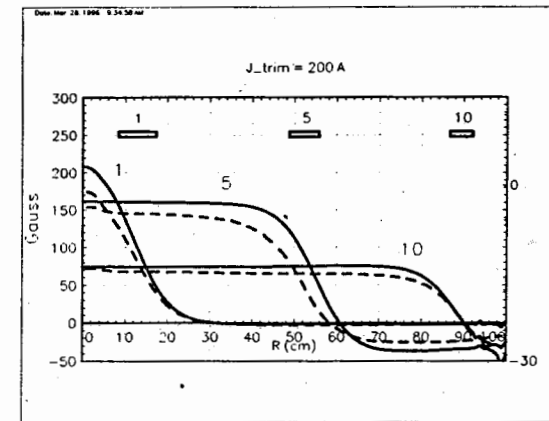

Figure 6: Trim coil mean field. The main coil current is 600 A. The dashed lines are the 3D method, the solid lines are the 2D method.

between the sector and the medial disk and (as for the real coil) only part of it can be seen from the midplane. Due to the 4-fold symmetry of the magnet pole the coil is replicated 4 times along the azimuthal position with the same sign of the current. Nevertheless, the so obtained coil system is still applicable for the purpose of the single coil field contribution cross-check.

The comparison of two methods shows rather good agreement. Thus, near the final radius the amplitudes of the first harmonic are coincident within 10 % there. One can conclude that it is quite sufficient to use the less time consuming method 1 to get the harmonic coil field contribution with the required accuracy.

Axial Channel Field. In general, the 3D calculations have confirmed the 2D results. Near the midplane and inside the channel the character of the 2D and 3D curves is similar. But in the air gap between the sectors and near the interface between the sectors and the medial disk the 3D field value is 2 % ÷ 12 % smaller than the 2D field value.

The most striking difference between these two methods was revealed in the stray field region outside the magnet. The 3D field is $\approx$ 2 times larger than the 2D field there. The stray field becomes to be about zero only at Z = 6.4 m ÷ 7.6 m instead of 3 m in the 2D case (see Fig. 7).

Ponderomotive Forces. The main coil forces were estimated with the help of the OPERA-3D postprocessor. The program integrates the body forces on the source conductors, using J × B formula. Each section of the conductor is represented by a set of 20 node finite elements. Gaussian quadrature integration with 8 points is used to calculate the forces.

Figure 6: Trim coil mean field. The main coil current is 600 A. The dashed lines are the 3D method, the solid lines are the 2D method.

between the sector and the medial disk and (as for the real coil) only part of it can be seen from the midplane. Due to the 4-fold symmetry of the magnet pole the coil is replicated 4 times along the azimuthal position with the same sign of the current. Nevertheless, the so obtained coil system is still applicable for the purpose of the single coil field contribution cross-check.

· The comparison of two methods shows rather good agreement. Thus, near the final radius the amplitudes of the first harmonic are coincident within 10 % there. One can conclude that it is quite sufficient to use the less time consuming method 1 to get the harmonic coil field contribution with the required accuracy.

Axial Channel Field. In general, the 3D calculations have confirmed the 2D results. Near the midplane and inside the channel the character of the 2D and 3D curves is similar. But in the air gap between the sectors and near the interface between the sectors and the medial disk the 3D field value is 2 % ÷ 12 % smaller than the 2D field value.

The most striking difference between these two methods was revealed in the stray field region outside the magnet. The 3D field is ≈ 2 times larger than the 2D field there. The stray field becomes to be about zero only at $Z = 6.4$ m ÷ 7.6 m instead of 3 m in the 2D case (see Fig. 7).

Ponderomotive Forces. The main coil forces were estimated with the help of the OPERA-3D postprocessor. The program integrates the body forces on the source conductors, using J × B formula. Each section of the conductor is represented by a set of 20 node finite elements. Gaussian quadrature integration with 8 points is used to calculate the forces.
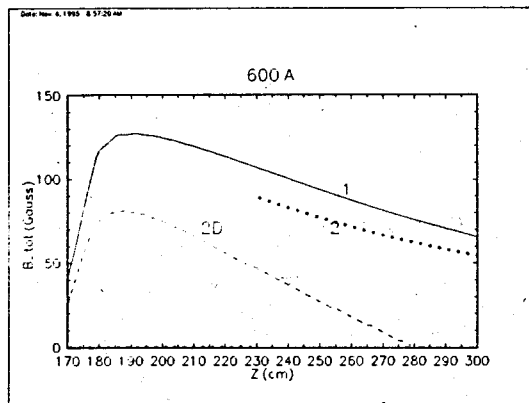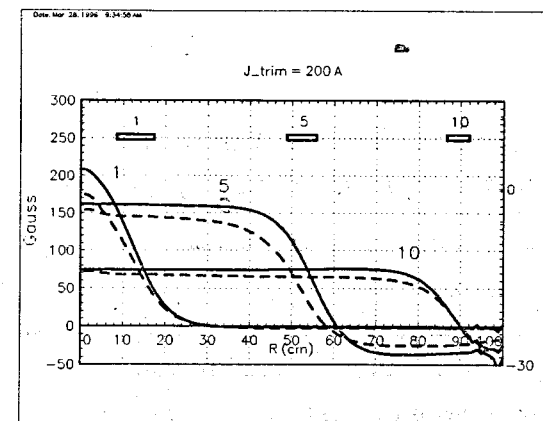
5

Figure 7: Stray field outside the magnet. 1 - integration method, 2 - nodal averaging method.

The results of the calculation are given in Fig. 8. The main coil current was 1000 A for the calculations. The comparison of the 3D and 2D calculations shows rather good agreement in the results.

In the 3D case one can notice the azimuthal variation of the forces along the coil length (variation range ≈ 40 %). This effect could be accounted for by the 2-fold yoke symmetry which provides less absolute value of the radial field gradient along the azimuths 90° and 270°, in between the magnet vertical yokes. The phenomenon, of course, cannot be detected with the 2D model, having in mind its cylindrical symmetry assumption.

The total force, acting on the half of one of the main coil pairs in the Y-direction, towards the vertical magnet yokes, is ≈ 82 kN. The analogous force outward the magnet, in the X-direction (in between the vertical yokes), is ≈ 74 kN.

The total force in the Z-direction on one of the main coil pairs is ≈ 178 kN in the 3D case, which can be compared with 187 kN for the 2D r-z model (≈ +5 % difference) and 170 kN for the 2D x-z model (≈ −4 % difference). This force tends to move the coil in the direction of the horizontal magnet yoke.

One can conclude that it is quite sufficient to use the less time consuming 2D method to calculate the forces, acting on the main coil, if the required accuracy would be ≈ ±20 % for the force density and ≈ ±5 % for the total force.

Conclusion. The 3D cross-check showed the satisfactory work of the 2D methods in the majority of the cases for the VINCY cyclotron magnet calculations, except the zero order harmonic, trim coil radial gradients, the stray field and ponderomotive force distributions.

Acknowledgment. The authors are pleased to express their thanks to Drs. P.Belicev,